

Thermal conductivity of perovskite KTaO_3 and PbTiO_3 from first principles

Yuhao Fu and David J. Singh

Department of Physics and Astronomy, University of Missouri, Columbia, MO 65211-7010, USA

(Dated: September 12, 2018)

The low thermal conductivity of piezoelectric perovskites is a challenge for high power transducer applications. We report first principles calculations of the thermal conductivity of ferroelectric PbTiO_3 and the cubic nearly ferroelectric perovskite KTaO_3 . The calculated thermal conductivity of PbTiO_3 is much lower than that of KTaO_3 in accord with experiment. Analysis of the results shows that the reason for the low thermal conductivity of PbTiO_3 is the presence of low frequency optical phonons associated with the polar modes. These are less dispersive in PbTiO_3 , leading to a large three phonon scattering phase space. These differences between the two materials are associated with the *A*-site driven ferroelectricity of PbTiO_3 in contrast to the *B*-site driven near ferroelectricity of KTaO_3 . The results are discussed in the context of modification of the thermal conductivity of electroactive materials.

I. INTRODUCTION

The low thermal conductivity of piezoelectric oxides, such as $\text{Pb}(\text{Zr,Ti})\text{O}_3$ (PZT) ceramics, limits the performance of high power transducers for applications such as sonar and ultrasonics. [1–4] It is also a constraint on emerging applications such as pyroelectric energy harvesting. [5] While this can be mitigated by careful design of the transducers, it is desirable to develop understanding of the low thermal conductivity of these materials, perhaps leading to modifications that can improve the heat conduction. Common PZT ceramics have ultralow thermal conductivities of $\kappa_l \sim 2$ W/mK or less at ambient temperature, decreasing with temperature to the ferroelectric phase transition, and then increasing sharply above the ferroelectric transition, [6] implying an association between the ultralow thermal conductivity and the ferroelectricity. It is also important to note that newer high performance materials, such as $\text{Pb}(\text{Mg}_{1/3}\text{Nb}_{2/3})\text{O}_3$ - PbTiO_3 alloy (PMN-PT) and $\text{Pb}(\text{Zn}_{1/3}\text{Nb}_{2/3})\text{O}_3$ - PbTiO_3 alloy (PZN-PT) piezocrystals have more strongly temperature dependent properties than PZT. This means that local heating may lead to strong changes in local dielectric and piezoelectric constants and resulting concentrations of electric field and mechanical stress potentially resulting in breakdown failure due to hotspots.

In other ferroelectric and near ferroelectric materials, particularly rocksalt structure chalcogenides, the interplay between polar transverse optical phonons and the longitudinal acoustic (LA) branch has been implicated in strongly lowering the thermal conductivity. [7–11] This is through a strong anharmonic coupling of the ferroelectric polar mode with the longitudinal acoustic mode, as seen directly in the very strong volume dependence of that mode, i.e. the high Grüneisen parameter. In addition, phase space considerations are important. [9–11]

Similarly, in perovskite ABO_3 ferroelectrics, there is typically a very strong pressure dependence to the polar mode and associated phase transitions, [12–15] indicating strong anharmonic coupling with longitudinal acoustic phonons near the zone center, where the LA modes are

compression waves.

This raises the questions of whether it is possible to have high thermal conductivity in a high performance perovskite piezoelectric, and if so how that might be achieved. Specifically, if ferroelectricity or proximity to ferroelectricity is the origin of the low thermal conductivity, and also is essential to the piezoelectric performance, it could be that low thermal conductivity is unavoidable. On the other hand, the perovskite structure is considerably more complex than the rocksalt structure, and mechanisms for ferroelectricity in perovskites are similarly more complex, which may provide avenues for increasing thermal conductivity that are not available in the nearly ferroelectric rocksalt compounds.

Here we report detailed first principles thermal conductivity calculations using solution of the Boltzmann-Peierls equation based on calculated three phonon anharmonic couplings for two prototypical materials with distinct behavior. These are PbTiO_3 , which is a high polarization ferroelectric that is the tetragonal end-member of the PZT solid solution, and KTaO_3 , which is a nearly ferroelectric perovskite with nearness to ferroelectricity coming from a different mechanism than in PbTiO_3 . Specifically, ferroelectricity is regarded as *A*-site (Pb) driven in PbTiO_3 but *B*-site (Ta) driven in the near ferroelectric KTaO_3 . [16] These two compounds have the advantages of representing different behaviors and having rather different experimental thermal conductivities, while retaining relatively simple five atom unit cells, which facilitates calculations and analysis. Additionally, there is high quality single crystal experimental thermal conductivity data available for these compounds. [17] We find that proximity to ferroelectric phase transitions is not the only factor in the thermal conductivity, but rather that the distinct phonon dispersions of *A*-site vs. *B*-site driven perovskites play a key role, suggesting possible avenues for improving the thermal conductivities.

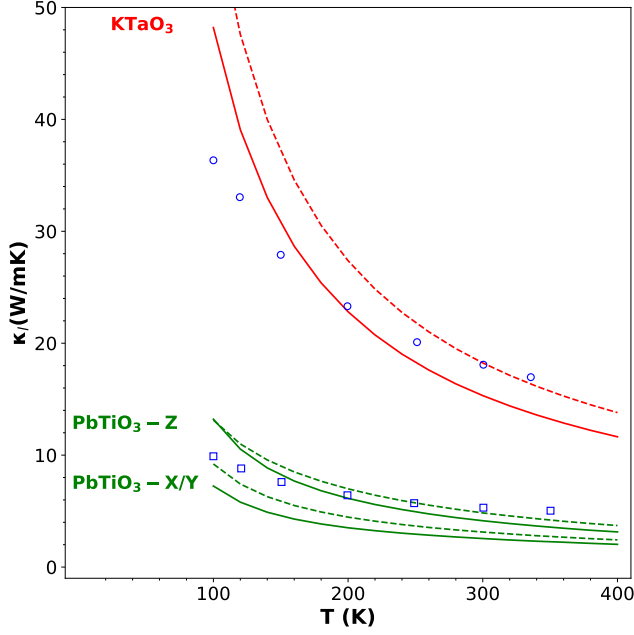


FIG. 1. Calculated temperature dependence of lattice thermal conductivity κ_l (in W/mK) of KTaO₃ and PbTiO₃. The solid lines indicate the κ_l for calculations with experimental lattice parameters, while the dashed lines indicate the κ_l with full relaxation including the lattice parameters. The experimental κ_l for KTaO₃ (open circles) and PbTiO₃ (open squares) are taken from Tachibana et al. [17].

II. COMPUTATIONAL METHODS

We performed first principles calculations of κ_l for perovskite KTaO₃ and PbTiO₃ in their ground state structures by iteratively solving the linearized Boltzmann-Peierls transport equation of phonons with the ShengBTE package. [18] Properties of ferroelectrics are often highly sensitive to the lattice parameters. We used the experimental values of the ambient temperature lattice parameters, [19, 20] and also did calculations with fully relaxed lattice parameters. The internal atomic positions were relaxed using total energy minimization. The experimental and calculated lattice parameters are $a=3.9883$ Å, and $a=3.9669$ Å, respectively, for KTaO₃ and $a=3.904$ Å, $c=4.1575$ Å, and $a=3.865$ Å, $c=4.036$ Å, respectively, for PbTiO₃. The interatomic force constants (IFCs) were obtained from density functional theory (DFT) calculations with the projector augmented wave (PAW) method [21], as implemented in the VASP code [22]. The 3p and 4s (K), 2p, 3d and 4s (Ti), 5p, 5d and 6s (Ta), 5d, 6s and 6p (Pb), 2s and 2p (O) electrons were treated explicitly as valence electrons. We used the local density approximation (LDA) for the exchange-correlation functional.

The kinetic energy cutoffs for the plane-wave basis set were set to 520 eV. The k-point meshes with grid spacing of $2\pi \times 0.03$ Å⁻¹ were used for electronic Brillouin

zone integration. Structural optimizations were done with a tolerance on residual forces of 10^{-4} eV/Å. The harmonic and third-order anharmonic IFCs were calculated by using the real-space supercell approach [18, 23] with a $3 \times 3 \times 3$ k-point mesh defining the supercells. The longitudinal optical - transverse optical (LO-TO) phonon splitting is large in these compounds, and was included using the dielectric constant and Born effective charges calculated from linear response density functional perturbation theory as implemented in the VASP code. Phonon momenta q -meshes of $15 \times 15 \times 15$ were used in solving the transport equation, which was sufficient to converge κ_l to a very high accuracy with respect to this parameter.

III. RESULTS AND DISCUSSION

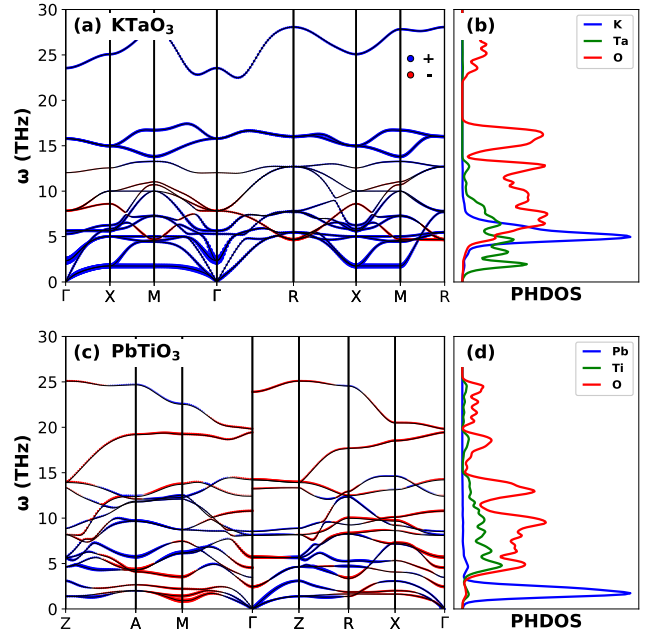


FIG. 2. (a, c) Calculated phonon dispersions of KTaO₃ and PbTiO₃. The symbol sizes give the Grüneisen parameter (γ) of each phonon mode. The colors, blue (+) and red (-) indicate positive and negative γ . The γ values of the lowest frequency phonons at M, X and R for KTaO₃ are 11.33, 12.03 and -3.19, respectively. For PbTiO₃, the γ values of the lowest frequency phonons at Z, A and M are 0.87, 0.20 and -14.45, respectively. The projected phonon densities of states (PHDOS) are shown in (b) and (d).

Our calculated thermal conductivity is shown in Fig. 1 along with comparison to experimental data in single crystals. [17] As seen, there is a very good agreement of the magnitude of the thermal conductivity with experiment, and in particular, the fact that KTaO₃ has a substantially higher thermal conductivity than PbTiO₃ is reproduced. The temperature dependence is, however, somewhat stronger in the calculated results than

TABLE I. Calculated lowest phonon frequencies at symmetry points, compared with experimental data. [24–27]

		Calc. (THz)	Exp. (THz, 300K)
KTaO₃	Γ	2.34	2.56 ^a
		5.63	6.24 ^a
		7.84	8.58 ^a
	M	1.76	1.82 ^b
		5.02	5.27 ^a
		10.00	10.28 ^a
	X	1.76	1.90 ^a
		5.01	5.22 ^a
		5.85	5.99 ^a
	R	4.66	4.90 ^a
		5.48	5.76 ^a
		7.69	7.63 ^a
PbTiO₃	Γ	2.45	2.61 ^c
		3.48	3.84 ^c
		4.55	4.47 ^c
	X	1.64	1.62 ^d
		2.01	1.97 ^d
		3.07	2.96 ^d

^aReference[24].

^bReference[25].

^cReference[26].

^dReference[27].

in experiment. One possible reason for this discrepancy may be that the low frequency phonons are temperature dependent in these materials, while we use the harmonic zero temperature frequencies in the calculations presented here. In any case, it is clear that the calculations do capture the large difference between PbTiO₃ and KTaO₃, which we discuss below, starting with the phonons.

The phonon dispersions and projected phonon densities of states of the two materials are given in Fig. 2. Grüneisen parameters, γ are indicated on the dispersions. Table I gives a comparison between calculated low frequency phonons and available experimental data. [24–27] Overall, we find very good agreement between our calculated phonon frequencies and experimental data. It should, however, be mentioned that the lowest mode at Γ in KTaO₃ is the soft mode, which is strongly temperature dependent; [28] for this mode, agreement with experiments done at 300 K is misleading; its frequency is overestimated in our calculations if one considers the temperature dependence.

In any case, as seen in the phonon dispersions, the two materials are very different. KTaO₃ has a low frequency two fold degenerate transverse optic mode at the zone center, as expected. This mode has a sizable positive Grüneisen parameter, implying strong anharmonic coupling to the longitudinal acoustic mode. It is associated with *B*-site (Ta) off-centering in its octahedral cage,

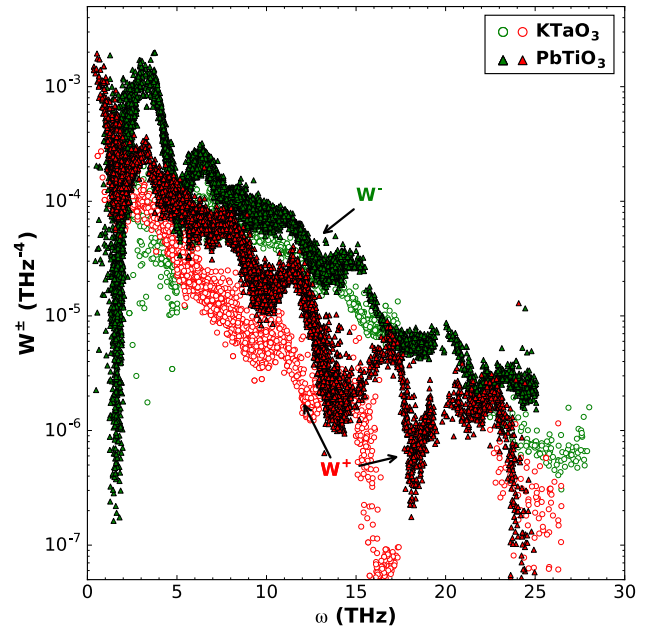


FIG. 3. Calculated three-phonon anharmonic scattering phase space (W^\pm) of KTaO₃ and PbTiO₃. The +(-) sign represents three-phonon absorption (emission) phase space. Note the log scale.

along with smaller *A*-site displacements. [29] This mode anti-crosses with the acoustic branches and remains low frequency in sheets around the Γ -X-M planes, i.e. the planes defined by $k_x=0$, $k_y=0$ or $k_z=0$. These phonons are not, however, low frequency elsewhere in the Brillouin zone, as seen from the dispersions along Γ -R, X-R and M-R. This sheet like structure of the regions of the zone where the *B*-site off-centering phonons are low frequency corresponds to the chain-like displacements noted in early diffuse scattering experiments for the *B*-site driven ferroelectrics, KNbO₃ and BaTiO₃. [30, 31]

The phonons of PbTiO₃ are very different, characteristic of *A*-site driven materials, [16] and consistent with prior calculations and experiment. [32–34] There is a prominent low frequency peak in the phonon density of states with strong *A*-site (Pb) participation. This comes off-centering polar modes, which are associated with the ferroelectricity. These have primary Pb character, and smaller cooperative Ti displacements, as typical for *A*-site driven ferroelectrics. [16] Also, different from KTaO₃ there are additional low frequency modes at the zone corners, M, corresponding to rotation of the TiO₆ octahedra. These modes have sizable negative Grüneisen parameter, meaning that they soften with lattice compression, characteristic of tilt modes in titanate perovskites. [13, 35, 36] Note that at the zone center the polar modes associated with Pb off-centering also have negative Grüneisen parameter. This is because pressure suppresses ferroelectricity, which for the already ferroelectric perovskite PbTiO₃ means pressure moves the system towards the

ferroelectric instability, and therefore softens the polar modes. Also, importantly, the Pb off-centering modes associated with ferroelectricity do not have the chain structure that is present in *B*-site driven perovskites. Instead they have low frequency throughout the Brillouin zone. These predominantly Pb modes underlie the low frequency peak in the phonon density of states. The key finding is that the main difference between the dynamics of PbTiO_3 and KNbO_3 is not in the anharmonicity, but is in the phonon dispersions.

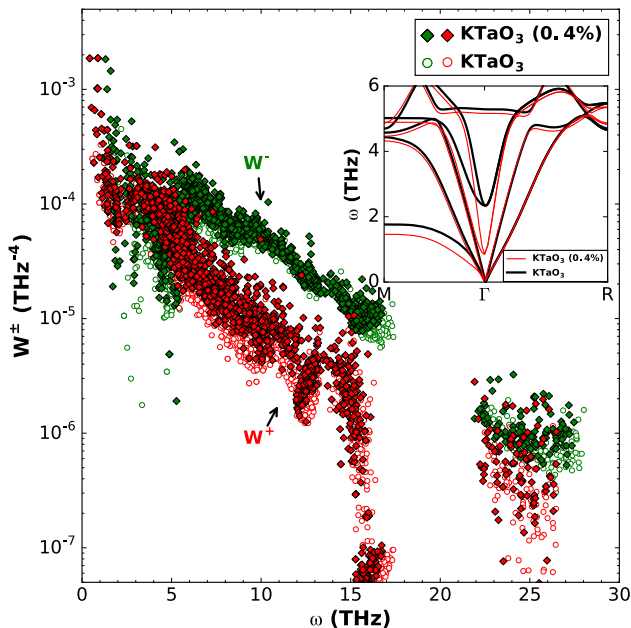


FIG. 4. Calculated three-phonon anharmonic scattering phase space (W^\pm) of KTaO_3 and KTaO_3 (0.4% of expansion in lattice parameters). The $+$ ($-$) sign represents three-phonon absorption (emission) process.

This is reflected in the scattering phase space. Fig. 3 shows the calculated three-phonon anharmonic absorption and emission phase space for the two compounds at the experimental lattice parameter. As seen, the scattering phase space is very much larger for PbTiO_3 than for KNbO_3 , including importantly the low frequency region below ~ 5 THz that is important for heat conduction. This explains the very low thermal conductivity of PbTiO_3 relative to KTaO_3 . In particular, the fact that in perovskite structure, the *A*-site motions are less correlated than the *B*-site motions in *B*-site driven materials, leads to flat low frequency branches associated with the polar mode, extending throughout the Brillouin zone. This provides a large phase space for anharmonic phonon scattering and thus low thermal conductivity.

We now turn to the issue of proximity to the ferroelectric instability. Fig. 4 shows the scattering phase space for KTaO_3 for two different lattice parameters, while the

inset shows the corresponding change in phonon dispersion. In KTaO_3 the volume expansion lowers the polar mode frequency bringing the material much closer to the ferroelectric instability. This is reflected in an increase in the scattering phase space at low frequency. However, the changes are modest compared to the large difference between PbTiO_3 and KTaO_3 .

The resulting reduction in calculated thermal conductivity at 300 K is from 15.3 W/mK to 11.1 W/mK, even though with the volume expansion the material is much closer to the ferroelectric instability as seen in the phonon dispersion. Thus, while proximity to ferroelectricity is important, it is not the main issue in the low thermal conductivity of PbTiO_3 , since the largest contribution to the scattering is not from the region of the zone very close to the Γ point.

IV. SUMMARY AND CONCLUSIONS

Thermal conductivity calculations show that the low thermal conductivity of PbTiO_3 in relation to KTaO_3 reflects the difference between *A*-site driven and *B*-site driven polar perovskite materials, and not the proximity to ferroelectricity. The implication is that it may be possible to find chemical modifications that maintain the electromechanical properties of piezoelectric perovskite ferroelectrics, while increasing the thermal conductivity. This understanding may also be of use in related materials classes, for example, in perovskite thermoelectrics related to SrTiO_3 , [37] where reduction of the thermal conductivity is desired, as is typically the case for thermoelectrics. [7, 38]

One strategy suggested by the present results may be to find chemical ways of increasing the coupling between *A*-site and *B*-site displacements. The rationale is that it is the correlation between *B*-site displacements that provides the dispersion of the low frequency polar modes in perovskites, as in the chain-correlations of KNbO_3 . This correlation between *B*-site displacements is usually understood as a consequence of covalency between the *B*-site and O, resulting in over- and under-bonding of O ions if the displacements are not coherent. [39, 40]

It will therefore be of interest to explore perovskite solid solutions based on *A*-site driven electroactive materials to find systems with enhanced coupling between *A*-site and *B*-site displacements and/or enhanced *B*-site – O covalency, to determine if thermal conductivity can be enhanced while retaining desirable piezoelectric properties. This may also lead to better control of thermal issues in applications and perhaps better control of breakdown issues in piezocrystals.

ACKNOWLEDGMENTS

We are grateful for a helpful discussion with Lane Martin.

-
- [1] F. B. Stulen, N. Senapati, and R. Gould, *Ultrasonics Int.* **83**, 301 (1983).
 - [2] J. N. Decarpigny, B. Hamonic, and O. B. Wilson, Jr., *IEEE Trans. Oceanic Eng.* **16**, 107 (1991).
 - [3] B. Dubus and D. Boucher, *J. Acoust. Soc. Am.* **95**, 1983 (1994).
 - [4] S. C. Butler and R. Montgomery, *J. Acoust. Soc. Am.* **105**, 1121 (1999).
 - [5] Q. Wang, C. R. Bowen, W. Lei, H. Zhang, B. Xie, S. Qiu, M. Y. Li, and S. Jiang, *J. Mater. Chem. A* **6**, 5040 (2018).
 - [6] S. N. Kallaev, G. G. Gadzhiev, I. K. Kamilov, Z. M. Omarov, S. A. Sadykov, and L. A. Reznichenko, *Phys. Solid State* **48**, 1169 (2006).
 - [7] O. Delaire, J. Ma, K. Marty, A. F. May, M. A. McGuire, M. H. Du, D. J. Singh, A. Podlesnyak, G. Ehlers, M. D. Lumsden, and B. C. Sales, *Nature Materials* **10**, 614 (2011).
 - [8] A. H. Romero, E. K. U. Gross, M. J. Verstraete, and O. Hellman, *Phys. Rev. B* **91**, 214310 (2015).
 - [9] C. W. Li, O. Hellman, J. Ma, A. F. May, H. B. Cao, X. Chen, A. D. Christianson, G. Ehlers, D. J. Singh, B. C. Sales, and O. Delaire, *Phys. Rev. Lett.* **112**, 175501 (2014).
 - [10] R. M. Murphy, E. D. Murray, S. Fahy, and I. Savic, *Phys. Rev. B* **93**, 104304 (2016).
 - [11] N. Shulumba, O. Hellman, and A. J. Minnich, *Phys. Rev. B* **95**, 014302 (2017).
 - [12] G. A. Samara, *Ferroelectrics* **2**, 277 (1971).
 - [13] M. Fornari and D. J. Singh, *Phys. Rev. B* **63**, 092101 (2001).
 - [14] A. Sani, B. Noheda, I. A. Kornev, L. Bellaiche, P. Bouverier, and J. Kreisel, *Phys. Rev. B* **69**, 020105 (2004).
 - [15] N. Jaouen, A. C. Dhaussy, J. P. Itie, A. Rogalev, S. Marinell, and Y. Joly, *Phys. Rev. B* **75**, 224115 (2007).
 - [16] M. Ghita, M. Fornari, D. J. Singh, and S. V. Halilov, *Phys. Rev. B* **72**, 054114 (2005).
 - [17] M. Tachibana, T. Kolodiazny, and E. Takayama-Muromachi, *Appl. Phys. Lett.* **93**, 092902 (2008).
 - [18] W. Li, J. Carrete, N. A. Katcho, and N. Mingo, *Comput. Phys.* **185**, 1747 (2014).
 - [19] E. A. Zhurova, V. E. Zavodnik, and V. G. Tsirel'son, *Crystallogr. Rep.* **40**, 753 (1995).
 - [20] J. Joseph, T. M. Vimala, V. Sivasubramanian, and V. R. K. Murthy, *J. Mater. Sci.* **35**, 1571 (2000).
 - [21] P. E. Blochl, *Phys. Rev. B* **50**, 17953 (1994).
 - [22] G. Kresse and J. Furthmüller, *Phys. Rev. B* **54**, 11169 (1996).
 - [23] A. Togo, F. Oba, and I. Tanaka, *Phys. Rev. B* **78**, 134106 (2008).
 - [24] G. Shirane, R. Nathans, and V. J. Minkiewicz, *Phys. Rev.* **157**, 396 (1967).
 - [25] R. Comès and G. Shirane, *Phys. Rev. B* **5**, 1886 (1972).
 - [26] C. M. Foster, Z. Li, M. Grimsditch, S.-K. Chan, and D. J. Lam, *Phys. Rev. B* **48**, 10160 (1993).
 - [27] J. Hlinka, M. Kempa, J. Kulda, P. Bourges, A. Kania, and J. Petzelt, *Phys. Rev. B* **73**, 140101 (2006).
 - [28] S. Glinsek, D. Nuzhnyy, J. Petzelt, B. Malik, S. Kamba, V. Bovtun, M. Kempa, V. Skoromets, P. Kuzel, I. Gregora, and M. Kosec, *J. App. Phys.* **111**, 104101 (2012).
 - [29] D. J. Singh, *Phys. Rev. B* **53**, 176 (1996).
 - [30] R. Comes, M. Lambert, and A. Guinier, *Solid State Commun.* **6**, 715 (1968).
 - [31] R. Yu and H. Krakauer, *Phys. Rev. Lett.* **74**, 4067 (1995).
 - [32] P. Ghosez, E. Cockayne, U. V. Waghmare, and K. M. Rabe, *Phys. Rev. B* **60**, 836 (1999).
 - [33] C. H. Perry, R. Currat, H. Buhay, R. M. Migoni, W. G. Stirling, and J. D. Axe, *Phys. Rev. B* **39**, 8666 (1989).
 - [34] I. Tomeno, Y. Ishii, Y. Tsunoda, and K. Oka, *Phys. Rev. B* **73**, 064116 (2006).
 - [35] M. A. Islam, J. M. Rondinelli, and J. E. Spanier, *J. Phys.: Condens. Matter* **25**, 175902 (2013).
 - [36] H. J. Xiang, M. Guennou, J. Iniguez, J. Kreisel, and L. Bellaiche, *Phys. Rev. B* **96**, 054102 (2017).
 - [37] J. Sun and D. J. Singh, *APL Mater.* **4**, 104803 (2016).
 - [38] G. Rogl and P. Rogl, *Materials Today Physics* **3**, 48 (2017).
 - [39] I. Grinberg, V. R. Cooper, and A. M. Rappe, *Phys. Rev. B* **69**, 144118 (2004).
 - [40] S. Liu, I. Grinberg, H. Takenaka, and A. M. Rappe, *Phys. Rev. B* **88**, 104102 (2013).